First Observations of Recurring HF-Enhanced Topside Ion Line Spectra Near the Fourth Gyroharmonic

Theresa Rexer[1] iD**, Björn Gustavsson[1]** iD**, Thomas Leyser[3]** iD**, Michael Rietveld[1,4]** iD**, Tim Yeoman[5]** iD**, and Tom Grydeland[2]** iD

[1]Institute for Physics and Technology, Arctic University of Norway UiT, Tromsø, Norway, [2]Northern Research Institute, Tromsø, Norway, [3]Swedish Institute of Space Physics, Uppsala, Sweden, [4]EISCAT Scientific Association, Ramfjordmoen, Norway, [5]Department of Physics and Astronomy, University of Leicester, Leicester, UK

Abstract We present first incoherent scatter radar observations of systematically recurring, high-frequency (HF)-enhanced ion line spectra at the topside F-region ionosphere, during magnetic field aligned HF pumping in an O-mode polarization. The European Incoherent Scatter UHF radar was directed in magnetic zenith on 9–11 March 2016 while stepping the pump frequency across the double resonance of the fourth harmonic of the electron gyrofrequency and the local upper hybrid frequency, in a 3-min-on, 3-min-off pump cycle. Topside and bottomside enhancements occur at the respective plasma resonance altitude and seem to be asymmetrically conditioned by the relative proximity of the pump frequency to the double resonance frequency. Further, the topside HF-induced ion line enhancements predominantly appear while the pump frequency is just below the double resonance frequency and only simultaneous to strong bottomside enhancements. A powerful, HF radio wave in O-mode, transmitted in the direction of magnetic zenith is reflected a few kilometers below the plasma resonance altitude, where the pump frequency is equal to the local plasma frequency, on the bottomside F-region in the ionosphere. Transionospheric propagation of the pump wave outside the radio window can be facilitated by density striations in the plasma, and we consider, in detail, the possible mechanisms proposed for propagation outside the standard radio window.

1. Introduction

A high-power, high-frequency (HF) O-mode radio wave with frequency lower than the peak ionospheric plasma frequency can drive a number of processes when it reaches the ionosphere. Depending on the power and polarization of the HF wave and the local plasma parameters, these include generation of small scale density depletions (e.g., Kelley et al., 1995; Honary et al., 1999), enhanced electron temperatures (e.g., Robinson et al., 1996; Rietveld et al., 2003), stimulated electromagnetic emissions at frequencies around the pump frequency (Leyser, 2001, and references therein) and enhanced optical emissions (e.g., Gustavsson et al., 2006; Kosch et al., 2002; Rietveld et al., 2003). Many of these responses vary in magnitude and character when the pump frequency, f_{HF}, varies, especially so when f_{HF} is close to a multiple, n, of the electron gyrofrequency, f_g, in the upper hybrid resonance layer. A vertically propagating, O-mode polarized pump wave has a reflection point, or cutoff, when it reaches an altitude where its frequency is equal to the local plasma frequency, f_P. Due to refraction in the ionosphere, rays at angles larger than the *Spitze* angle (equation (1)) will reflect at slightly lower altitudes (Rietveld et al., 1993). Signatures of pump wave propagation beyond the reflection height to higher altitudes and regions of higher plasma frequency and density was first observed in ionograms (Ellis, 1956). In incoherent scatter radar (ISR) measurements, effects of the HF pump wave above the O-mode reflection height were first observed at midlatitudes (Ganguly & Gordon, 1983) and later at high latitudes (Isham et al., 1990). For this to occur, certain conditions have to be met.

An O-mode pump wave propagating in a strictly field aligned direction, $\mathbf{k}\|\mathbf{B_0}$ and $\mathbf{k}_\perp = 0$, is a left-hand circular polarized (LHCP) wave, and at the point where $f_p = f_{HF}$, it can pass trough a narrow ($\sim 1°$) radio window (Mjølhus, 1990). This limiting case of a wave that is strictly field aligned is known as an L-mode wave (Chen, 1983). For altitudes where the pump frequency is higher than the local plasma frequency, $f_{HF} > f_p$, the wave is in LHCP O-mode with the corresponding dispersion relation, while for altitudes where the pump frequency is lower than the local plasma frequency, $f_{HF} < f_p$ it is a LHCP X-mode wave (see Figure 1 in

Nordblad & Leyser, 2010). The X-mode branch of the L-mode wave is also known as the Z-mode (Mjølhus, 1990), but the Z-mode usually refers to all wave vectors from parallel to perpendicular to the magnetic field. The standard radio window for an O-mode pump wave is at the *Spitze* angle,

$$\sin(\theta_c) = \sin(\alpha)\sqrt{\frac{Y}{1+Y}} \tag{1}$$

with $Y = \frac{f_g}{f_{HF}}$ and α is the angle of the magnetic field from vertical, in a horizontally stratified ionosphere (Budden, 1980). The *Spitze* angle is that angle of incidence for which an O-mode wave, transmitted from the ground, has refracted to being magnetic field aligned (**k** ∥ **B$_0$**) when reaching the plasma resonance height. At the European Incoherent Scatter (EISCAT) facility in Tromsø the radio window is between $\theta_c = 5°-6°$ south from vertical, depending on the pump frequency (Isham et al., 1996).

Four possible mechanisms for propagation of a pump wave beyond the reflection height, outside of this narrow radio window, have been proposed. The first is the introduction of new artificial radio windows by large-scale density striations in the ionosphere that guide an O-mode wave such that the transmission conditions are met outside the standard radio window (Leyser & Nordblad, 2009; Nordblad & Leyser, 2010). Such density ducts, with horizontal scales on the order of a kilometer, can exist naturally (e.g., Fejer & Kelley, 1980; Gurevich et al., 1995) or can be efficiently generated by the O-mode HF pump wave (Gurevich et al., 1998; Kelley et al., 1995; Leyser & Wong, 2009; Utlaut & Violette, 1974, and references therein). If the propagating wave does not encounter the L-mode cutoff at,

$$f_{HF} = f_L = -\frac{f_g}{2} + \frac{1}{2}\sqrt{f_g^2 + 4f_p^2} \tag{2}$$

after passing through a radio window, it continues propagating to higher altitudes and can reach the topside ionosphere (Eliasson et al., 2012; Mjølhus & Flå, 1984), and continue to propagate into space (Leyser et al., 2018).

The second mechanism is a resonant scattering process of the pump wave on small-scale, field aligned, density irregularities (Mishin et al., 2001). Here the incident O-mode pump wave can efficiently be transformed in to a Z-mode wave as a result of scattering on the field aligned striations at the bottomside ionosphere. As the propagating wave reaches the topside, several turbulent processes may occur and transform the wave to O-mode and electrostatic waves at this altitude. The small-scale density striations are strongly excited by the resonance instability (Vas'kov & Gurevich, 1977), and models for their nonlinear stabilization have been obtained (Gurevich et al., 1995; Istomin & Leyser, 1997).

Eliasson (2008) has simulated a propagation process for low duty-cycle experiments, minimizing the effect of density irregularities, with vertically propagating O-mode waves. Here the incident O-mode wave is efficiently converted to Z-mode waves within a few milliseconds, due to Langmuir turbulence, at the reflection altitude. The Z-mode wave will propagate to higher altitudes and reach the topside reflection altitude. This mechanism is effective only for low duty cycles and pump waves that reach the resonance altitude, and thus not a probable explanation for the observational results of our experiment.

A fourth mechanism for producing topside enhancements at midlatitudes (Vas'kov et al., 1995) has been proposed by Vodyanitskij et al. (1974), in which resonant electrons at the bottomside, exited by the pump wave, carry the plasma oscillations to the topside ionosphere. We consider this effect to be unlikely for our observations due to the large distance between the top and bottomside ionosphere. Neither thermal- nor photo-electrons have a long enough mean-free-path length (∼ 4, 2.5, and 10 km at 220 km for 1, 10, and 100 eV, respectively) to reach the topside F-region with flux modulated by the pump frequency, at the bottomside ionosphere resonance altitude.

Enhancements of the backscattered power in the ion and plasma lines of ISR measurements in the ionosphere, due to high-power HF wave pumping, have been observed many times (e.g., Ganguly & Gordon, 1983; Isham et al., 1990; Isham, Rietveld, et al. 1999; Isham, Hagfors, et al. 1999; Kosch et al., 2011; Rietveld et al., 2002). Isham et al. (1990) reported ion-line enhancements at the topside and bottomside of the F-region observable during the first 10-s period after heating on in magnetic zenith. During their experiment, topside HF ion line enhancements (THFIL) were sporadically observed from one heating on pulse to the next. In 1997, Isham, Rietveld, et al. (1999) performed a second experiment where THFIL were clearly seen in the data from
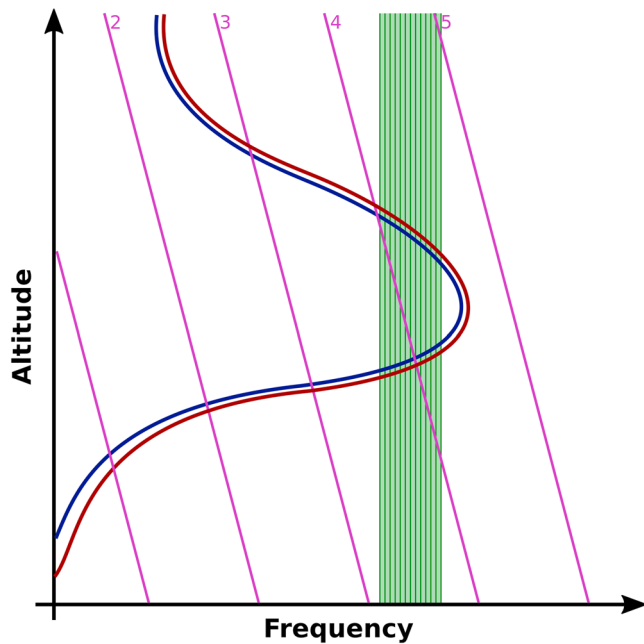
Figure 1. Schematic of the experiment setup. Red and blue lines illustrate the altitude profile of the local upper hybrid- and plasma frequency, respectively. Pink diagonal lines show harmonics of the electron gyrofrequency, while the green shaded area indicates the frequency range in which the HF pump wave stepped.

both the UHF and VHF radar at the EISCAT site in Tromsø. Again, observations showed clear THFIL and the the authors attribute the observations to a coupling of the O-mode wave to the Z-mode at the altitude where $f_p = f_{HF}$ and the pump wave is parallel to the magnetic field, $\mathbf{k} \parallel \mathbf{B_0}$, that is, the radio window. Mishin et al. (2001) suggested the resonant scatter process of the pump wave, facilitating a conversion from O-mode to Z-mode waves on small-scale field-aligned irregularities as the cause for these observations. Nordblad and Leyser (2010) also suggest that L-mode propagation through heater induced radio windows can not be ruled out as an explanation for the Isham, Rietveld, et al. (1999) observations. In an experiment studying the angular extent of the radio window in 2004, Kosch et al. (2011) observed clear topside enhancements during a low duty cycle (3.3%), heating experiment pointed in a direction 9° south of zenith. They present observations indicating the location of the bottomside radio window to be around 7°–8° south of zenith, arguing that this can be explained by a tilt in the ionosphere, that was observed in the Dynasonde data during the experiment. Interestingly, they observe the equatorward, 2°–3°, displacement of the topside enhancements relative to the bottomside radio window, first predicted by Mjølhus and Flå (1984). Most recently, Leyser et al. (2018) presented possible evidence of L-mode propagation through the F-region, where $f_{OF2} > f_{HF}$, into space.

In this paper we present first observations of systematically occurring HF-enhanced ion line spectra from the topside ionosphere when stepping through the fourth electron gyroharmonic frequency. During a heating experiment on 9–11 March 2016 at the EISCAT facility near Tromsø, Norway, clear THFIL from the F-region were observed in 33 out of 90 heating on pulses. The HF pump frequency of each on pulse was stepped through the fourth harmonic of the electron gyrofrequency. Observations of the natural ionospheric Langmuir waves, enhanced by photo electrons during daytime conditions, in the plasma line spectra of the UHF radar have been used to calculate the electron density giving the critical plasma frequencies in the ionosphere with an unprecedented accuracy. This allows us to determine that THFIL occur in the plasma resonance region where, $f_p = f_{HF}$, in the ionosphere. A gyro harmonic effect of the THFIL and bottomside ion line enhancements (BHFIL) was detected, when the pump frequency was near the double resonance of the local upper hybrid frequency and the fourth harmonic of the electron gyrofrequency. The upper hybrid resonance region has been studied extensively, and the "double resonance" frequencies of the different electron gyro harmonics have been shown to be of great importance and is the focus of a large body of research (see, e.g., Ashrafi et al., 2007; Borisova et al., 2014; Dhillon & Robinson, 2005; Grach et al., 2016; Gustavsson et al., 2006; Honary et al., 1995; Honary et al., 1999; Kosch et al., 2002; Leyser et al., 1989; Stubbe et al., 1994; Robinson et al., 1996, and references therein).

We present the first observations of topside HF-enhanced ion line spectra, as well as first experimental results of a gyro harmonic effect of the enhancements. All topside enhancements are compared and analyzed in the context of the critical plasma frequencies in the ionosphere.

2. EISCAT Heating and UHF Radar

On 9–11 March 2016 EISCAT Heating (Rietveld et al., 2016) was operated in a 3-min-on, 3-min-off cycle, transmitting LHCP HF radio waves in the magnetic zenith direction, which upon reaching the ionosphere have most of their energy in the O-mode. The experiments were conducted during quiet geomagnetic daytime conditions from 10:00 UT to 13:00 UT on all 3 days. During the 3-min-on pulse, the pump frequency, f_{HF}, was kept constant for 1 min, then increased in steps of 10 or 20 kHz every 10 s for 2 min. The pump frequency was chosen such that it was stepped through the double resonance of the local upper hybrid frequency, f_{uh}, and the fourth harmonic of the electron gyrofrequency, $4f_g$, such that the condition

$$f_{HF} = f_{uh} = 4f_g \tag{3}$$

was met at some point in the bottomside ionosphere, during the frequency stepping. Here $f_{uh}^2 = f_g^2 + f_p^2$. The effective radiated power (ERP) on 9 March was 359 MW at 5.35 MHz O-mode heating with 12.5 MW X-mode
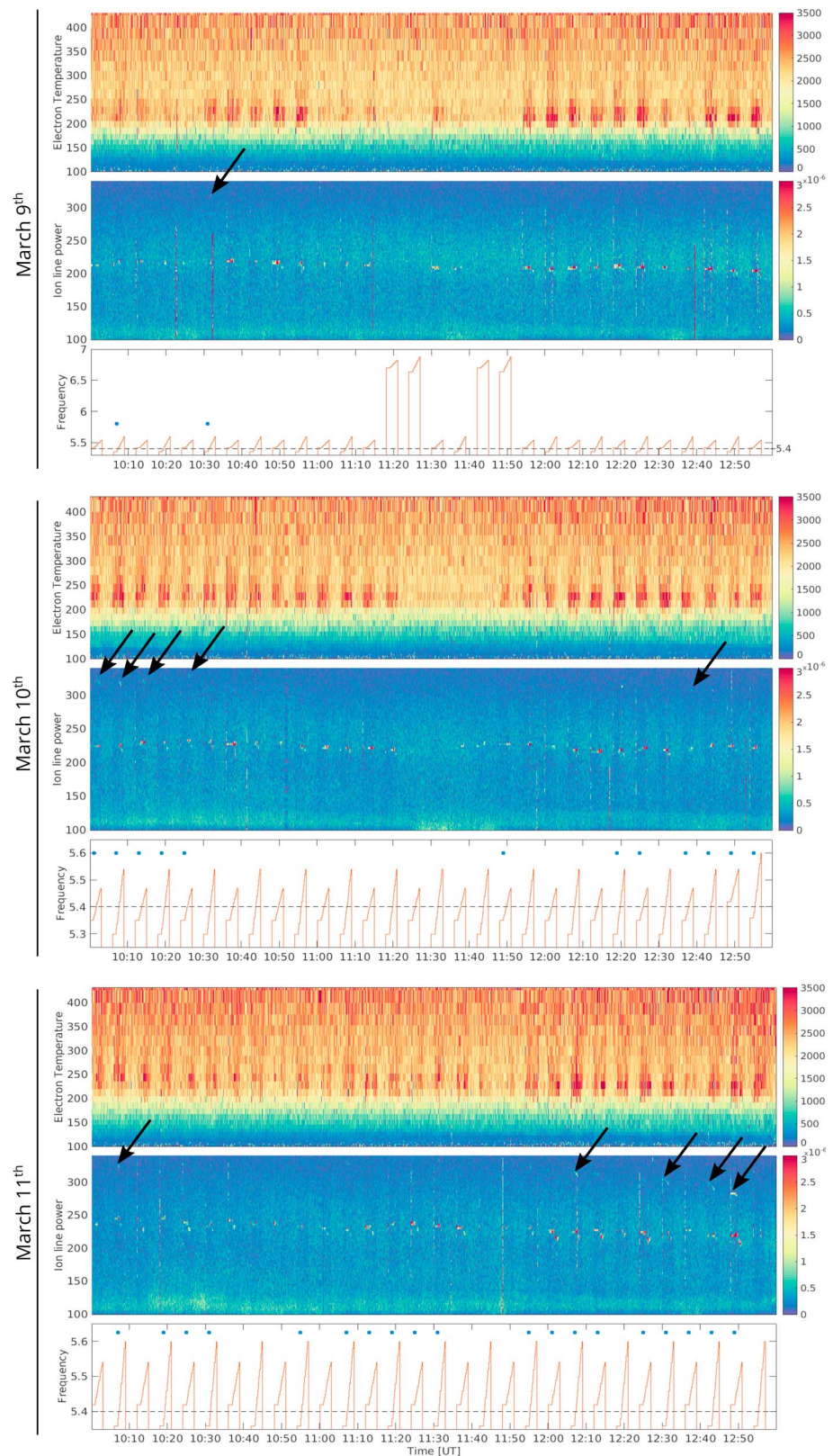
Figure 2. Electron temperature (top), backscattered ion line power (middle) and pump frequency (bottom) for 9–11 March 2016. Blue dots in the bottom panels indicate heating pulses during which topside ion line enhancements are observed. Black arrows highlight some, but not all, enhanced backscatter in the ion line power at the topside ionosphere.
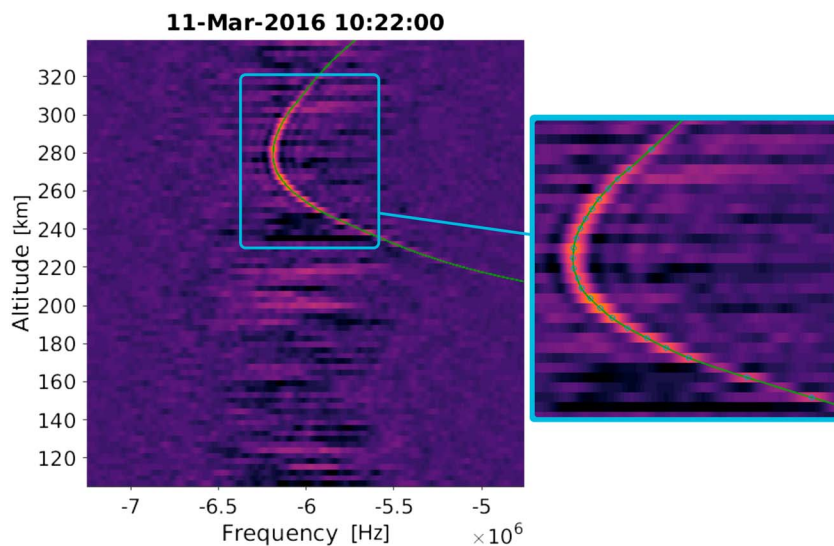
Figure 3. Example of a 1-min integrated and low-pass-filtered plasma line spectra data from 11 March 2016 at 10:22 UT, which is used to calculate a curve fit to the natural Langmuir wave enhancements. Blue circles indicate signals that are 5 standard deviations above noise level, which are used to find the fit shown in green.

"leakage" and a beamwidth of 7.0° in the north-south plane. On 10 March the ERP of the heater was 330 MW at 5.35 MHz, with a beamwidth of 7.2°, while on 11 March, the ERP was 363 MW at 5.42 MHz, and the beamwidth was 7.0°.

A schematic of the experiment setup is shown in Figure 1, where the red and blue lines illustrate the altitude profile of the upper hybrid and plasma frequency. Gyrofrequency harmonics are sketched in pink, and the frequency band in which we step the HF pump wave is shown in green to give an overview of important frequencies involved in the experiment and their relation. From this illustration we see that for a portion of each 3-min-on pulse, the pump frequency will be just below and just above the double resonance frequency, as we step through it by increasing the pump frequency.

The ionospheric response of the HF modulation wave was observed using the colocated EISCAT UHF radar, also pointing in the direction along the local magnetic field. The IS-radar measurements were done with the "beata" program (see Lehtinen & Huuskonen, 1996; Tjulin, 2017, and references therein). Only lags out to 410 μs are computed, which gives a frequency resolution of 2.4 kHz. Range gates are computed from 49 to 693 km of range, with 5-s temporal resolution and 3-km range resolution. In addition, the plasma line is sampled at 0.4 μs, covering a 2.5-MHz wide band offset from the transmit frequency by 8.4, 6, and 3.4 MHz, and covering ranges from 107 to 374 km. During the experiment strong backscatter from the natural existing Langmuir waves in the ionosphere were observed, mostly in the −6 MHz band of the downshifted plasma spectra.

Figure 2 shows summary plots of the experiment and results from 10:00 UT to 13:00 UT for 9 (top), 10 (middle), and 11 (bottom) March 2016. The upper panel for each day shows the electron temperature modulated by the HF pumping. The response in the backscattered power of the ion line is shown in the second panel. Arrows indicate some, but not all, examples of the strongest THFIL backscatter we observe, which are apparent even in these overview figures. In the bottom panel the heating on/off times and frequency are shown. Blue dots indicate all HF pump pulses where clear topside ion line enhancements are found during the analysis. Several plasma line spectra are observed, where strong enhancements at different frequencies and altitudes, coincidental with the HF pump wave. These are not discussed in detail in this paper.

3. Determination of Electron Density From Plasma Line Frequency Spectra

From the downshifted UHF power spectra it was possible to identify the frequency of peak power from the backscatter of natural Langmuir waves in range gates from about 180 to 320 km. This made it possible to obtain an accurate estimate of the electron density. From the Langmuir wave altitude profile we calculate the electron density, adapting the relevant parts of the method for temperature determination from plasma line
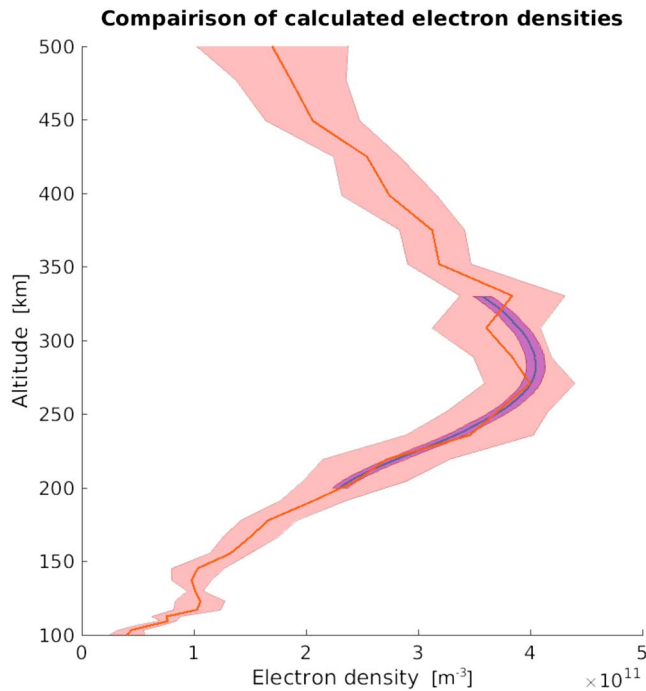
Compairison of calculated electron densities

Figure 4. Altitude profile of electron density calculated during heating off from the ion line and plasma line spectra obtained from the UHF EISCAT radar on 11 March 2016 at 10:17:00 UT. The red shaded area shows the 1σ uncertainty level for the ion line density calculations, while the blue area shows the reasonable uncertainty for the electron density as calculated from the plasma line.

observation described by Hagfors and Lehtinen (1981). Solving the dispersion relation for the downshifted plasma line, f_-, for the density, N_e we obtain the physically relevant solution:

$$N_e = \left(\frac{m_e \epsilon_0}{q^2}\right) \left[\frac{-y + \sqrt{y^2 - 4xz}}{2x}\right]^2 \qquad (4)$$

where

$$x = \frac{1}{2\pi} + \frac{3T_e}{4m_e \pi c^2}, \qquad y = f_- - \frac{6T_e f_0}{c^2 m_e}, \qquad z = \frac{12\pi T_e f_0^2}{c^2 m_e}$$

where f_0 is the UHF radar frequency and c the speed of light. T_e and m_e are the electron temperature and mass respectively.

We used standard ISR parameters estimated from 30 s integrated ion line data for the electron temperature, necessary for these calculations. Although the altitude resolution of this electron temperature data is the same as for the estimated electron density parameter, obtained from the ion line, N_e is weakly dependent on T_e. Thus, T_e only contributes with a small correction term to N_e in equation (4). The densities obtained from this calculation are used to calculate O-, X-, and L-mode cutoff frequencies and the plasma- and upper hybrid- frequency, which are used in the analyses presented in this paper.

An example of 1-min integrated and low-pass-filtered, plasma spectra from 100 to 340 km, between −7.25 and −4.75 MHz, on 11 March 2016 at 10:22 UT are shown in Figure 3. The green line indicates the calculated curve fit to the signal of the natural Langmuir waves. Backscatter from the natural Langmuir waves are clearly visible for 80–90 km in altitude around the F-layer maximum frequency, around 280 km. Weaker backscatter from these is distinguishable well above the background noise, also for altitudes down to around 220 km and up to around 320 km, for this time interval. For most spectra from this experiment, the range where a clear power enhancements from Langmuir waves was detected was between 180 and 320 km and for frequencies below −5.25 MHz. The curve fit in frequency and altitude is obtained from signals where the power enhancements are 5 standard deviations or more above the mean noise level, at that altitude.

Previously, the electron densities have been obtained from ion-acoustic waves detected in the ion line spectra of the EISCAT radar. The altitude resolution obtained through this method decreases with height and is ≈20–25 km around 150–350 km, and hence, the accuracy and precision of the densities calculated from these is restricted. In Figure 4 we compare the altitude profile of the electron density as calculated from the ion and plasma line on 11 March 2016 at 10:17:00 UT. The red shaded area indicates 1 standard deviation for the ion line density data as calculated from the same time interval as was used for the curve fit to the natural Langmuir wave enhancements in the plasma line. The blue shaded area indicates the uncertainty of the electron density calculated from the plasma line. This uncertainty was obtained by combining 1 standard deviation for the temperature, σ_{T_e}, with an assumed frequency uncertainty, σ_f, of 20 kHz, which corresponds to the mean half width, half maximum of the power enhancement signals of the plasma line. Comparing the altitude resolution and the calculated accuracy of these, as in the example in Figure 4, it is clear that the densities calculated by this method, from the natural Langmuir wave signatures observed in the plasma spectra, improve our results significantly for the altitudes where naturally enhanced plasma line data are available.

4. Data Analyses and Results

We now look at the observations made by the UHF radar during the frequency stepping of the pump wave, focusing only on the 3-min-on pulses where we observe topside enhancements of the ion line spectra. Clear topside enhancements were detected during 33 heating on pulses on 9–11 March 2016. The examples of the enhancements on the topside ionosphere shown in the following section are all from separate heating on pulses, in order to emphasize and demonstrate the systematic occurrence of the THFIL with respect to the double resonance frequency.
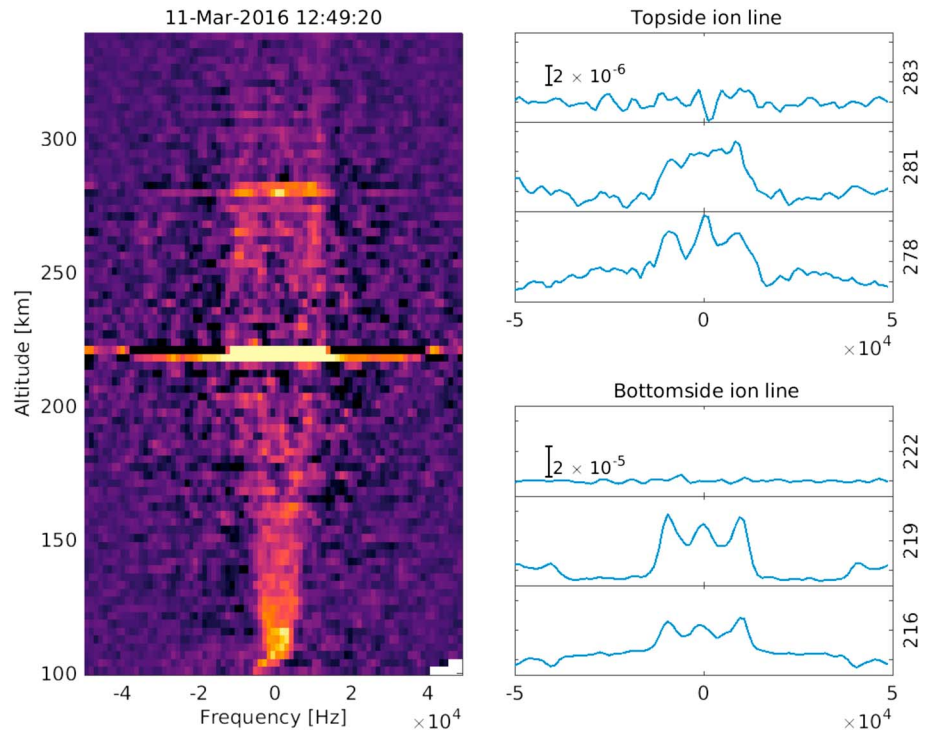
Figure 5. Example of an ion spectra showing topside enhancements on 11 March at 12:49:20 UT (left). The top and bottom panels on the right show the line spectra at the altitude of the strongest enhancements for the top and bottomside ionosphere, respectively.

Figure 5 shows a typical example of the ion line enhancements from 12:49:20 on 11 March at the instant during the on pulse where the topside enhancement is the strongest. The figure shows the first published observations of the THFIL spectra. The left panel shows an instant in time, of the backscattered power in the ion spectra range, where the bottom and topside enhancements are clearly visible during HF pumping. The upper and lower right panel show line plots, of the same spectra as in the left panel, at the altitude of the strongest enhancement for the topside and bottomside, respectively. Note that the scales of the line plots for the topside and bottomside enhancement are different and that the backscattered power from the topside is weaker by an order of magnitude. We observe this difference in backscattered power for most pulses. Signatures of the natural ion line spectra are seen at all altitudes. To isolate the HF-enhanced backscatter, the
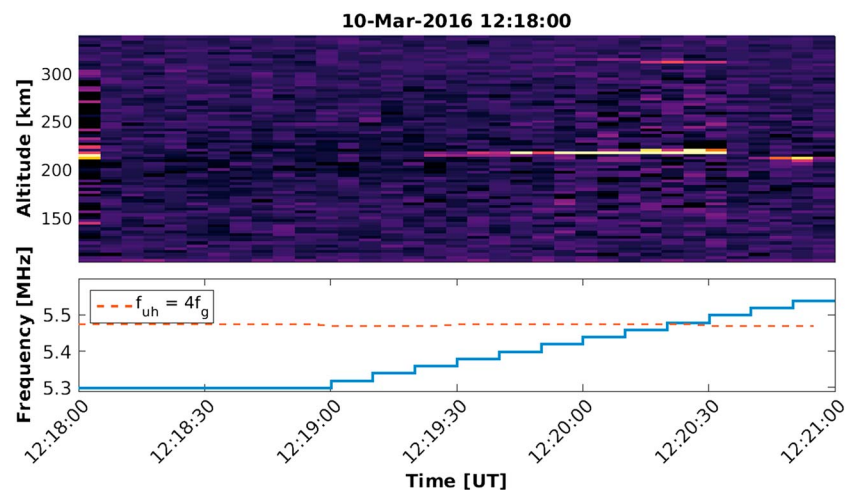

Figure 6. The time evolution of the averaged backscattered power in the ion line spectra for one 3-min-on pulse from 10 March at 12:18 UT. The bottom panel shows the pump frequency and double resonance frequency.
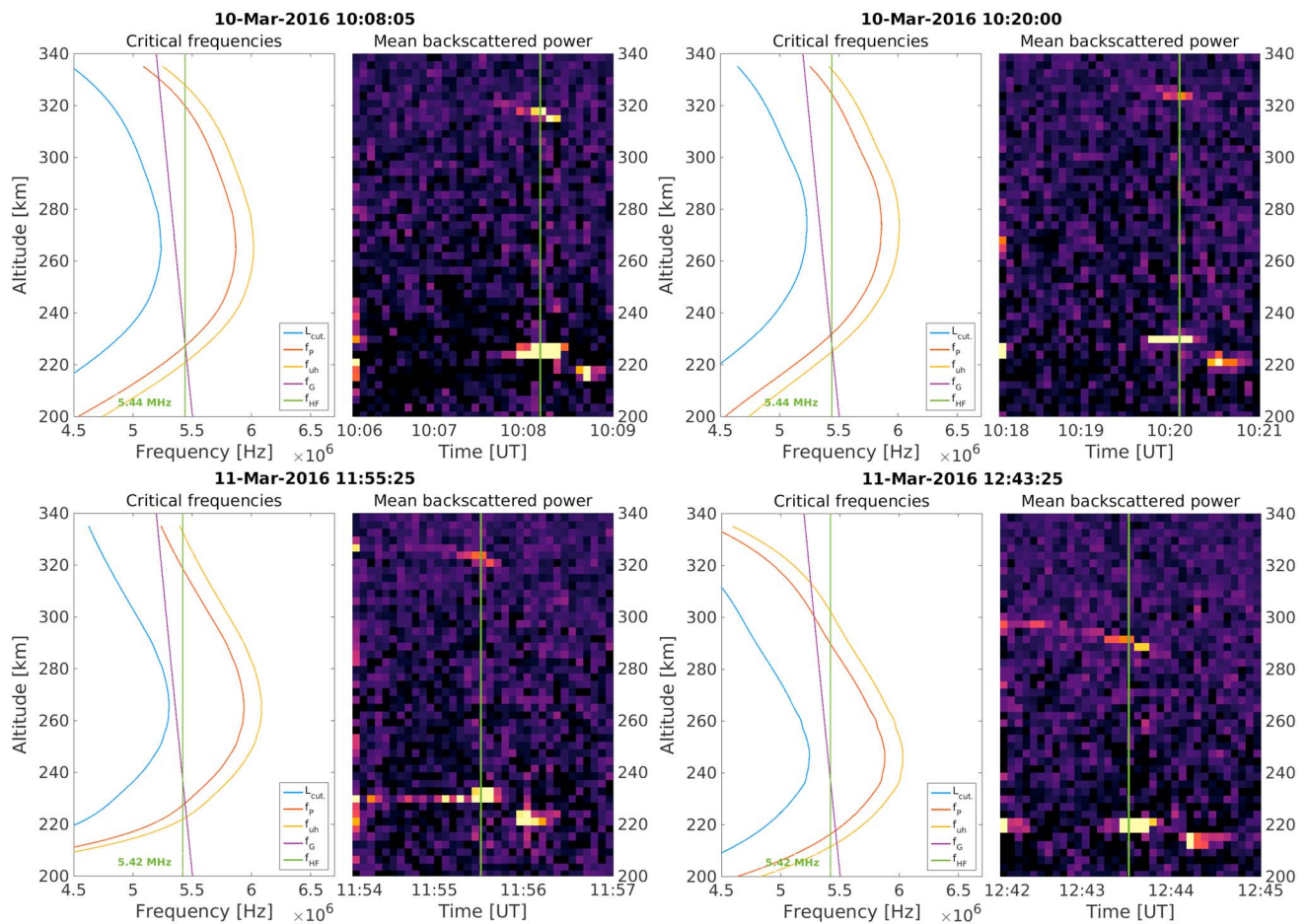
Figure 7. Four examples of 3-min pulses where we see clear topside enhancements. The left plot in each panel shows the critical frequencies calculated from the observed natural Langmuir waves. The blue line indicates the L-mode cutoff (equation (2)), the red is the local plasma frequency, purple shows the fourth harmonic of the electron gyrofrequency, while the green vertical line indicates the frequency of the transmitted O-mode pump wave. Right panel shows the 5-s mean backscattered ion line power during a 3-min-on pulse. The vertical green line indicates the time corresponding to the left panel plot.

natural ion line backscatter is calculated from a 1-min heating off period immediately before start of a new heating on period and subtracted from all ion spectra in the following 3 min of heating on. This background subtraction is done for all following ion spectra presented here.

Figure 6 shows the temporal evolution of the mean, 5-s integrated, ion line power during the on pulse starting at 12:18:00 UT on 11 March. The transmitted pump frequency is indicated in blue in the lower panel along with the frequency of the double resonance in red. The overshoot effect (Stubbe, 1996) is apparent in the first 5 s of the heating on period. Starting at 12:19:20 UT in the 213-km altitude range gate, the BHFIL is clearly seen until 12:20:35 UT where the strongest enhancement is in the 222-km altitude range gate. The topside enhancement, for this pulse, appears weakly first at 12:20:05 UT at 316 km and is visible for 30 s until 12:20:35 UT, where it is strongest at 310 km. The altitude resolution of the radar in this experiment is around 3 km so the respective decrease and increase in the altitude of the strongest THFIL and BHFIL corresponds to 3 and 2 steps in altitude. That is ∼9 and ∼6 km, respectively. The increase and decrease of altitude of the enhancements is consistent with the respective increase and decrease of the resonance altitude, where $f_P = f_{HF}$, as we step the pump frequency up during the 3-min pulse, and we observe this in most pulses. At the time of the appearance of the first bottomside enhancement, the pump frequency is 5.36 MHz. At 12:20:40 UT, where both topside and bottomside enhancements abruptly disappear the pump frequency is 5.5 MHz after having been stepped every 10 s in 20-kHz increments. A second bottomside enhancement appears at 12:20:45 UT in the 210-km range gate and lasts for 15 s before the pump is turned off.

Four further examples, out of the 33 pulses with clear THFIL observations, are shown in Figure 7. All left-hand plots show the altitude profile of the critical frequencies, f_p, f_{UH}, $4f_g$, and the L-mode cutoff frequency
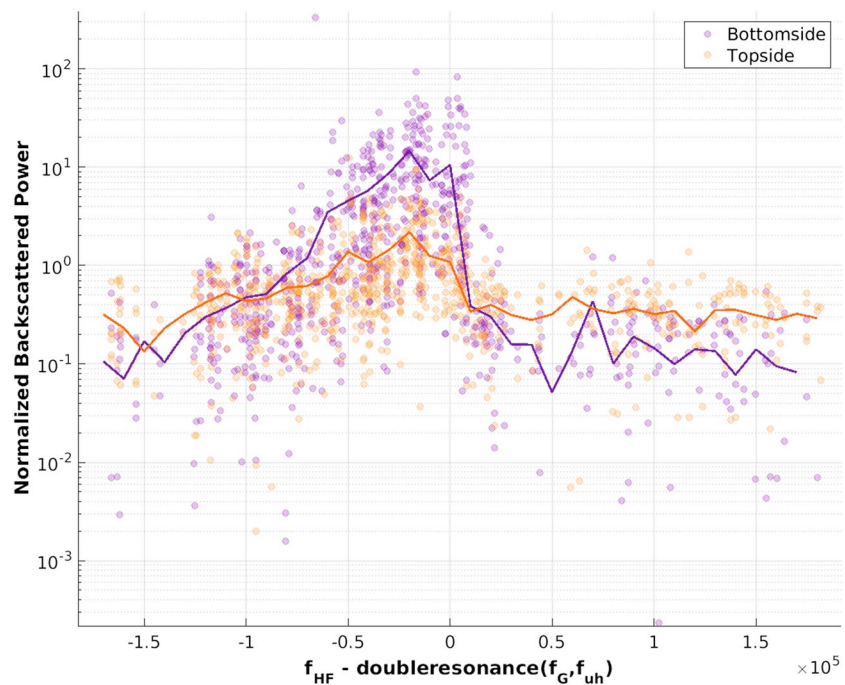
Figure 8. Comparison of all 33 heating pulses. Backscattered ion line power relative to the difference of the pump and double resonance frequency. Topside enhancements are shown in orange while bottomside enhancements are shown in purple. The superposed lines show the mean of the observation.

(equation (2)) calculated from enhanced backscatter from natural Langmuir waves observed in the plasma line of the radar (see section 3). The green number toward the bottom of the plot indicates the pump frequency at this instant. The corresponding right plots, as in Figure 6, show the temporal evolution of the mean backscattered power from −15 to 15 kHz, in the ion line for the 3-min HF on period, with the time indicated on the x-axis. The vertical green line indicates the time of the strongest backscatter from the THFIL, to which the left plot corresponds for each pulse.

For all 33 pulses with identified THFIL we see consistent responses. This is seen in Figure 8 where we compare the normalized backscattered power of all data points of the 33 pulses, at the altitude of the strongest BHFIL and THFIL. We relate this, to the difference between the pump frequency and the double resonance frequency, that is, how close the HF pump frequency is to the double resonance. Negative values indicate an HF pump just below the double resonance frequency. BHFIL are shown in violet, while the THFIL are orange. The mean of these observations is shown by the solid lines in the same color coding. Comparing these and illustrated by the four pulses shown in Figure 7, we observe the following similarities for THFIL:

1. Signatures of the overshoot effect are easily identified in the first 5-s integration period after heating on, as seen in the four right-hand plots of Figure 7.
2. After the overshoot with the pump frequency still kept constant, very little or no enhancement of backscattered power is seen.
3. As the HF pump frequency is increased throughout the pulse the BHFIL intensity increase until they reach a maximum and decrease significantly, then disappear completely (Figure 8).
4. Simultaneous to the increase in the BHFIL we observe clear enhancements at the topside ionosphere.
5. The strongest backscatter from the THFIL coincides with the strongest backscatter from the BHFIL.
6. For the two pulses shown in the bottom panels of Figure 7 we can recognize a THFIL also before the strongest BHFIL, while for the two pulses in top panels, the THFIL seems to appear simultaneous to the strongest BHFIL.
7. A decrease and increase of altitude of the THFIL and BHFIL, respectively, is clearly visible in the figure and corresponds to the increasing altitudes of resonance for increasing f_{HF}.
8. Comparing this observation to the left plots of Figure 7, which all show the critical frequencies calculated for the instant at which the strongest THFIL is observed, in all panels, we see that the BHFIL and THFIL occur close
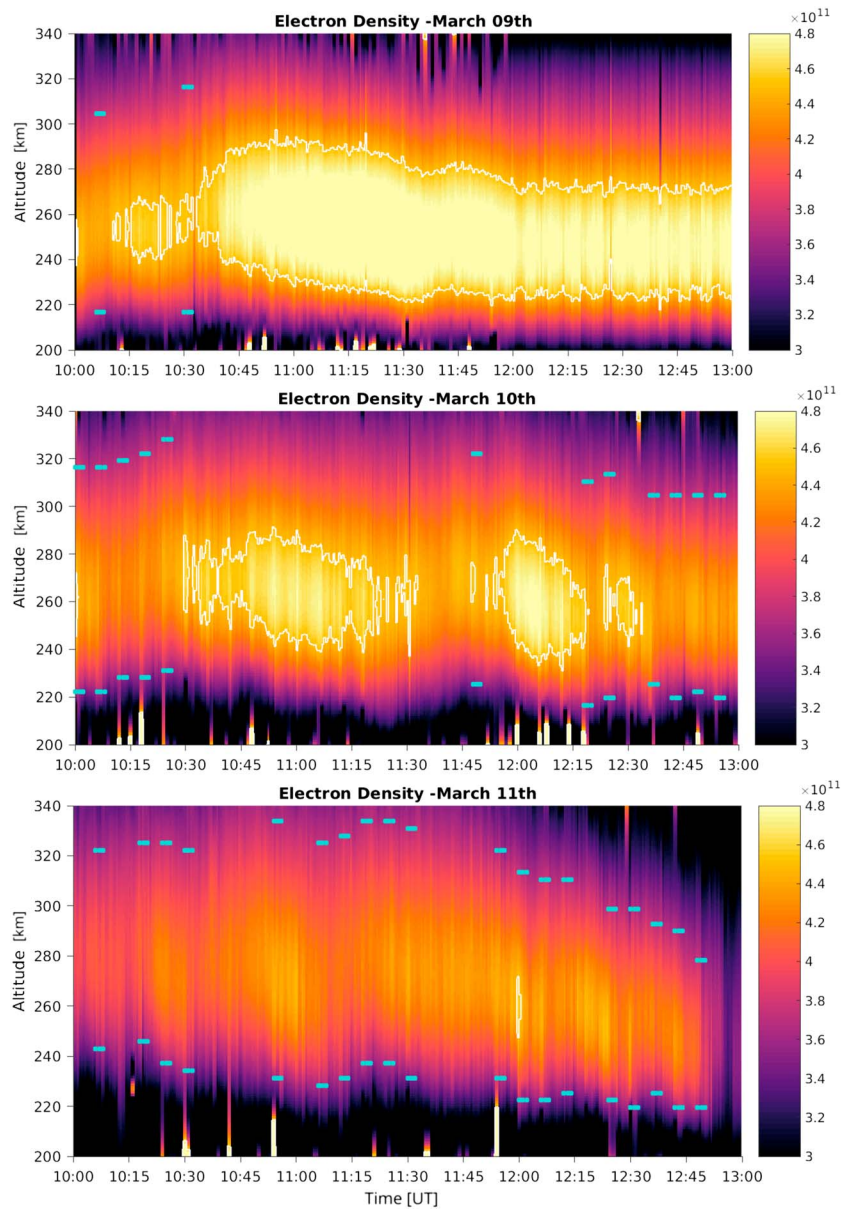
Figure 9. Electron density (color) calculated from the UHF plasma line observations of the natural Langmuir wave enhancements on 9–11 March 2016. A white contour indicates the superposed L-mode cutoff frequency of 5.4 MHz, and the altitude and occurrence of BHFIL and THFIL for pulses where THFIL are observed are shown by blue bars.

to the altitude where the HF pump frequency (green) is equal (or close to) the the local plasma frequency f_P (red) at the topside and bottomside ionosphere.

9. The second BHFIL, appearing at lower altitudes, is seen for all of the shown pulses after the main BHFIL.

The electron density at altitudes from 200 to 340 km, for the duration of the experiment on all 3 days is shown in Figure 9. As for Figure 7, the density is calculated as described in section 3. Blue bars show the altitude and time of the BHFIL and THFIL for all pulses where THFIL where observed. The white contour in these three figures indicates where the L-mode cutoff frequency (see equation (2)) is 5.4 MHz and is intended to give an indication of when the cutoff frequency was close to or at the pump frequency. In the bottom panels for all days in Figure 2 we have marked this frequency, for comparison to the pump frequency, by the dashed line. For three heating on pulses with observed THFIL (9 March at 10:30 UT and 10 March at 12:18 UT and 12:24 UT), the pump frequency is below the L-mode cutoff for the beginning of the pulse. As we step the pump frequency up, it increases above the local L-mode cutoff frequency toward the end of the heating pulse,
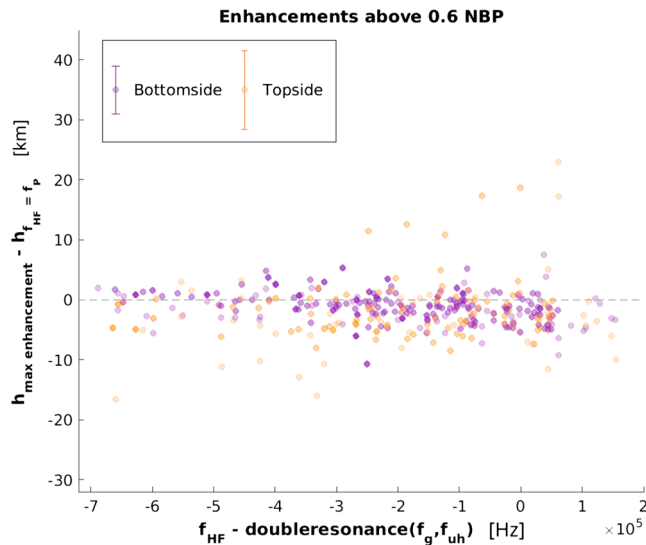
Figure 10. Comparison of the altitude of the appearance of the THFIL and BHFIL above 0.6 NBP in the ion line spectra, and the altitude of the plasma resonance, $f_P = f_{HF}$ as calculated from the plasma line. The mean error of ± 4 km for the bottomside and ± 6.6 km, for for the topside, for all points is indicated in the legend.

permitting trans-ionospheric propagation. It is nevertheless evident in Figure 9 that THFIL is generally only observed when the L-mode cutoff is sufficiently low, that is, below the frequency at which the pump wave can propagate as an L-mode wave without encountering a cutoff. In this figure we also see that the altitude of the observed BHFIL and THFIL fluctuates with the observed density variations on all 3 days.

The altitude of the observed enhancements and the altitude of the resonance heights, $f_p = f_{HF}$ at the top and bottomside ionosphere, obtained from the calculations discussed in section 3, is shown in Figure 10. The altitude of data points, where the normalized backscattered power is stronger than 0.6, is compared to the altitude of the resonance height, at that time, for the THFIL and BHFIL separately. It is clear from the figure that the enhancements at both altitudes occur at or close to, their respective resonance heights. Mean errors of ± 4 and ± 6.6 km, indicated in the figure, for the bottomside and topside altitudes, respectively, are due to the uncertainty in the plasma line fit and the difference in temporal resolution of the plasma line fit and the ion line spectra. The discrepancy in the temporal resolution also accounts for the slight negative trend of the altitude differences.

5. Discussion

We present the first observations of THFIL spectra from EISCAT UHF radar measurements during HF modulation experiments. The EISCAT Heating facilities transmitted a LHCP electromagnetic wave into the ionosphere directed in magnetic zenith, in a 3-min-on, 3-min-off cycle while stepping the pump frequency across the double resonance frequency at the fourth gyroharmonic. The different aspects of the observations are discussed systematically in the following.

5.1. Appearance of THFIL

Thirty-three cases of THFILs are clearly identified in our observations during HF-pumping with frequency stepping through the double resonance frequency. In Figure 9 the altitude of the THFIL and BHFIL for all 33 pulses are indicated. It is clear that no THFIL are observed when electron densities are high enough, such that there is a cutoff for the L-mode waves at f_{HF}. We see that the altitudes of both the THFIL and the BHFIL match the plasma resonance altitude of $f_p = f_{HF}$.

As apparent, from Figure 9, there are a number of heating on pulses (14) on 10 and 11 March, where no THFIL are observed, even though the L(Z)-mode cutoff frequency is lower than the pump frequency. On 10 March the L(Z)-mode cutoff frequency is below the double resonance frequency, from 11:30 UT to 11:51 UT, but only for the last (starting at 11:48 UT), of the four on pulses transmitted during that period, do we observe topside enhancements. Comparing the electron temperature during this period, shown in the middle panel of Figure 2, we see no temperature enhancements during these heating pulses. However, we do see an increased backscattered power in the ion line around 100-km altitude, in the middle panel, possibly due to E-region absorption. As a result of partial absorption at lower altitudes, less HF-wave power reaches the F-region and we observe very weak or no BHFIL for those three pulses.

On 11 March, 11 HF pulses were transmitted (10:00, 10:12, 10:36, 10:42, 10:48, 11:00, 11:36, 11:42, 11:48, 12:18, and 12:54 UT), where no THFIL were observed. For four of these (10:12, 10:42, 11:36, 12:18 UT), faint traces of THFIL can perhaps be detected. However, these were very weak and below the threshold we set for THFIL and were thus not included in our analysis. Noticeably the backscattered power of the ion line and temperature modulations (see bottom panels Figure 2), on the bottomside ionosphere for these four pulses was much lower than for pulses with observed THFIL enhancements. For the pulses at 10:36, 11:00, 11:42, and 11:48 UT we observed significantly weaker BHFIL than for pulses with THFIL. The electron temperature enhancements shown in Figure 2, during these pulses are also lower then for other pulses. Figure 8 indicates that THFIL primarily occur simultaneously to the BHFIL enhancements. It seems likely that there exists a threshold that has to be exceeded, such that a large enough fraction of wave energy can propagate beyond the bottomside reflection height and that this was not achieved during the pulses where the BHFIL were weak.

For the absence of the THFIL enhancement in the remaining three pulses, there are several possible explanations. The lack of a THFIL from the HF pulses starting 10:00 and 10:48 UT on 11 March are particularly interesting as they had an initial frequency of 5.42 MHz closely matching our estimate of the double resonance frequency for that time. For the pulse at 10:48 UT we initially observe clear BHFIL for 1 min, but no THFIL. For the pulse at 10:00 UT, no HFIL at any altitude was observed until the pump frequency was well above the double resonance.

Generation of density striations is significantly reduced for HF-pumping at the double resonance frequency. If propagation to the topside ionosphere is facilitated by small- or large-scale density striations in the ionospheric plasma, generated by the pump wave, then no THFIL are expected for this pulse. This could indicate that some period of heating on, at a frequency where small- or large-scale striations are effectively generated, is necessary prior to pumping at the double resonance frequency, were less wave energy is absorbed by turbulent upper hybrid processes such that the wave can propagate further. Further experiments are required to clarify this.

For the last HF pulse transmitted on 11 March at 12:54 UT, the electron density in the ionosphere had decreased such that the double resonance frequency was below the lowest pump frequency.

5.2. Evolution of THFIL

Four conclusions can be drawn from Figure 8:

1. Enhancements are observed when the pump frequency is between ∼ 80 kHz below the double resonance frequency and ∼ 9.8 kHz above the double resonance frequency.
2. All pulses have a similar development of the enhancements in relation to the relative proximity of the HF pump wave to the double resonance.
3. BHFIL are stronger than THFIL, sometimes up to an order of magnitude.
4. THFIL predominantly occur when we observe BHFIL.

A likely interpretation of the development of the observations is the following. During the first 5 s after heating on we observe the overshoot effect in all pulses, consistent with previous observations (e.g., Fejer, 1979; Honary et al., 1999; Showen & Behnke, 1978), which is rapidly suppressed within a few seconds, as the HF wave energy is absorbed through other processes (Robinson, 1989). Small-scale field-aligned striations are generated within a few seconds, as the HF pump wave is converted to UH electrostatic waves perpendicular to the geomagnetic field, at the upper hybrid resonance height (Robinson, 1989). Throughout this process no, or very little, enhanced ion acoustic or Langmuir waves are observed as most of the pump energy is absorbed by upper hybrid turbulence, leading to the formation of the density striations (e.g., Stubbe et al., 1994; Thidé et al., 2005), and significantly less reaches the resonance altitude.

As a result of the linear dispersion properties of upper hybrid waves around harmonics of the electron gyrofrequency, the growth of striations diminishes as the HF pump approaches the double resonance frequency (Mjølhus, 1993; Huang & Kuo, 1994; Robinson et al., 1996; Honary et al., 1999). The HF-pump energy can then be guided by the density irregularities and reach the resonance altitude, where coupling to Langmuir and ion acoustic waves is possible. This manifests itself, in the presented data, in the increase in ion line backscattered power on the bottomside ionosphere as the HF pump frequency approaches the double resonance. The enhancements increase while approaching the double resonance and abruptly disappear when the HF pump frequency increases beyond this, mirroring the asymmetric properties of the upper hybrid mode about the double resonance. Although the backscattered power of the THFIL is significantly less than that of the BHFIL, the THFIL show the same behavior as the BHFIL on approach of the double resonance as is seen in Figure 8.

5.3. Position and Altitude of the THFIL

As mentioned, there are two possibilities proposed for propagation of the incident wave to the topside ionosphere. The wave can pass through a radio window (Mjølhus, 1990), or the wave can be transformed into a Z-mode through the resonant scatter process (Mishin et al., 2001). While artificial, heater-induced radio windows can exist at multiple angles (Nordblad & Leyser, 2010), the standard radio window in a horizontally stratified ionosphere is located at the Spitze angle, around ∼5°–6° at EISCAT depending on the pump frequency (Isham et al., 1996).

Both the heater and the UHF radar were pointed in the magnetic field-aligned direction, at 12° south of zenith, for our experiment. This is well outside of the standard radio window at ∼ 6° at EISCAT. The heating beam at full width, half maximum (FWHM) for this experiment was ∼ 7°, such that angles from ∼ 9° to ∼ 16° were

effectively illuminated by the beam. Kosch et al. (2011) report observations showing the radio window appearing around 7°–8° with a spatial extent of 2° and a corresponding topside enhancement displaced further south by 2°–3°, appearing around 8°–12° and with and angular extent of 2°–3°. As their experiment was run with a very low-duty cycle (3.3%), minimizing the generation of pump-induced striations, they attribute this southward displacement of the standard radio window to a local tilt in the ionosphere.

The heating beam in our experiment does not extend far enough at FWHM, to reach the radio window observed by Kosch et al. (2011) at 7°–8°, but it is possible that parts of the beam at lower ERP do extend to this angle and propagate though the radio window. In this case the ionospheric tilt would have to be somewhat comparable to the tilt observed by Kosch et al. (2011). Also, as we observe topside enhancements multiple times on three consecutive days, any tilt during our experiment would have to occur systematically on all days and for the duration of all pulses where we do observe THFIL, in the same direction and with similar magnitude. In Figure 9, we see that the density varies considerably throughout the 3 hr on all 3 days. Especially on 10 and 11 March, we see signatures of periodic electron density variations. These variations are on timescales on the order of 10–40 mins, matching that of atmospheric gravity waves or traveling ionospheric disturbances (Hunsucker, 1982).

During our experiment the THFIL seem to occur independent of tilt angle when studying the five consecutive pulses on 11 March starting at 11:06:00 UT. Here we observe THFIL enhancement for every HF pulse while the electron density varies from high, $\sim 4.3 \times 10^{11}$ (lower altitude BHFIL), to low, $\sim 3.5 \times 10^{11}$, and back to higher density, possibly indicating a large-scale TID moving past the radar beam. During that period the ionospheric tilt angle would vary between opposites. Based on these considerations, we argue that it is unlikely that the propagation of the HF pump wave to the topside ionosphere occurs though the standard radio window but rather is a result of one of the proposed mechanisms for propagation outside the radio window.

Supporting our interpretation of the evolution of the THFIL observations (see section 5.2), and consistent with simulations done by Eliasson (2008), Figures 7 and 10 show that the altitude of both enhancements is at or close to the respective topside and bottomside plasma resonance altitude where $f_P = f_{HF}$. This is consistent with the shape of the enhanced ion line spectra of which we show examples for one instant in time, in the left panels of Figure 5. Two well-developed shoulders are observed in the ion line spectra at the altitudes of strongest enhancements of the topside and bottomside ionosphere, at 278 and 219 km, respectively. A prominent central feature characteristic for the oscillating two stream instability (e.g., Stubbe et al., 1992; Stubbe, 1996) is also visible for both enhancements. We observe the corresponding enhancement just below the pump wave frequency, in the plasma line spectrum at the bottomside ionosphere (not shown).

5.4. Propagation Outside the Radio Window

For both Z-mode scattering (Mishin et al., 2001) and L-mode propagation through artificial radio windows (Nordblad & Leyser, 2010), field-aligned electron density striations are essential for wave propagation outside the standard radio window. The resonant scatter process proposed by Mishin et al. (2001) should be effective when small-scale density irregularities are present at the reflection height of the pump wave. Small-scale density striations, on the order of several meters, are rapidly generated within a few seconds (Basu et al., 1997), by the pump wave itself and thus there is no "buildup" time or very little delay from heating on to the possible occurrence of THFIL. The characteristic timescales in the case of the L-mode propagation though artificially generated radio windows depends on the temporal evolution of kilometer-scale density striations. The L-mode wave is guided by large-scale density ducts that can be generated by the pump wave. Generation of large-scale density ducts is on the order of minutes (Basu et al., 1997).

Considering, as an example, the four pulses shown in Figure 7, we see that the two pulses from 10 March (top) are slightly different from the two bottom panel examples from 11 March. The temporal evolution of the two top panels is consistent with the generation of large-scale density striations facilitating L-mode propagation in artificial radio windows (Nordblad & Leyser, 2010), while the observations shown in the bottom panels are consistent with the Z-mode scattering process (Mishin et al., 2001). If large-scale density ducts exist before heating on, possibly from a previous heating on pulse, L-mode propagation is possible immediately. As exemplified in Figure 7, it is not unambiguously clear which of the two mechanisms is dominating from the observation made during our experiment. However, the topside enhancements were the strongest for pump frequencies near the double resonance (see Figure 8). It may be noted that for such conditions excitation of small-scale density striations is suppressed (Honary et al., 1999). This would thus also suppress the scattering of the pump wave into the Z-mode. As larger-scale ducts have a longer lifetime than small-scale striations

these may still facilitate guiding of the pump wave in the L-mode during the time near double resonance. Further, as the anomalous absorption of the pump wave is minimum at the double resonance (Stubbe et al., 1994), this may explain why the THFIL are the strongest for such frequencies. Further experiments are needed to study the physics involved.

6. Summary and Conclusions

We have shown systematically recurring ion line enhancements appearing at the topside ionospheric plasma resonance altitude, in the polar ionosphere on the three consecutive days, from 9 to 11 March 2016. These are the first observations of HF-enhanced ion line spectra at the topside ionosphere. The enhancements present evidence of radio wave propagation outside the standard radio window (∼ 6°) during O-mode, HF radio wave pumping along the local geomagnetic field (∼ 12°). Stepping the pump frequency across the double resonance of the fourth harmonic of the electron gyrofrequency and the local upper hybrid frequency, the enhancements seem to be asymmetrically conditioned by the relative proximity of the HF-pump frequency to the double resonance. THFILs predominantly appear while the HF-pump frequency is just below or at the double resonance frequency and the L-mode cutoff frequency is below the pump frequency. Approaching the double resonance frequency by the HF-pump frequency, the backscattered power of the THFIL and BHFIL increases until both enhancements abruptly disappear completely when the HF-pump frequency is larger than the double resonance frequency. Further, the THFIL only appear simultaneous to strong bottomside enhancements. We have considered the possible mechanisms proposed for radio wave propagation outside the standard radio window in detail. However, further experiments are needed to determine the dominating processes involved in HF pump wave propagation beyond the reflection height outside the radio window.

References

Ashrafi, M., Kosch, M. J., Kaila, K., & Isham, B. (2007). Spatiotemporal evolution of radio wave pump-induced ionospheric phenomena near the fourth electron gyroharmonic. *Journal of Geophysical Research*, *112*, A05314. https://doi.org/10.1029/2006JA011938

Basu, S., Costa, E., Livingston, R. C., Groves, K. M., & Carlson, H. C. (1997). Evolution of subkilometer scale ionospheric irregularities generated by high-power HF waves. *Journal of Geophysical Research*, *102*(A4), 7469–7475.

Borisova, T. D., Blagoveshchenskaya, N. F., Kalishin, A. S., Kosch, M. J., Senior, A., Rietveld, M., et al. (2014). Phenomena in the high-latitude ionospheric F region induced by a HF heater wave at frequencies near the fourth electron gyroharmonic. *Radiophysics and Quantum Electronics*, *57*(1), 1–19.

Budden, K. G. (1980). The theory of radio windows in the ionosphere and magnetosphere. *Journal of Atmospheric and Terrestrial Physics*, *42*(3), 287–298. https://doi.org/10.1016/0021-9169(80)90036-7

Chen, F. (1983). *Introduction to Plasma Physics and Controlled Fusion* (2nd ed.). Los Angeles, CA: Electrical Engineering Department School of Engineering and Applied Science University of California, Los Angeles.

Dhillon, R. S., & Robinson, T. R. (2005). Observations of time dependence and aspect sensitivity of regions of enhanced UHF backscatter associated with RF heating. *Annales Geophysicae*, *23*(1), 75–85. https://doi.org/10.5194/angeo-23-75-2005

Eliasson, B. (2008). Full-scale simulation study of the generation of topside ionospheric turbulence using a generalized Zakharov model. *Geophysical Research Letters*, *35*, L11104. https://doi.org/10.1029/2008GL033866

Eliasson, B., Shao, X., Milikh, G., Mishin, E. V., & Papadopoulos, K. (2012). Numerical modeling of artificial ionospheric layers driven by high-power HF heating. *Journal of Geophysical Research*, *117*, A10321. https://doi.org/10.1029/2012JA018105

Ellis, G. R. (1956). The Z propagation hole in the ionosphere. *Journal of Atmospheric and Terrestrial Physics*, *8*, 43–54.

Fejer, J. A. (1979). Ionospheric modification and parametric instabilities. *Reviews of Geophysics*, *17*(1), 135–153. https://doi.org/10.1029/RG017i001p00135

Fejer, B., & Kelley, C. (1980). Ionospheric Irregularities. *Reviews of Geophysics*, *18*(2), 401–454.

Ganguly, S., & Gordon, W. E. (1983). Heater enhanced topside plasma line. *Geophysical Research Letters*, *10*(10), 977–978.

Grach, S., Sergeev, E., Mishin, E., & Shindin, A. V. (2016). Dynamic properties of ionospheric plasma turbulence driven by high-power high-frequency radiowaves. *Uspekhi Fizicheskih Nauk*, *186*(11), 1189–1228. https://doi.org/10.3367/UFNr.2016.07.037868

Gurevich, A., Hagfors, T., Carlson, H., Karashtin, A., & Zybin, K. (1998). Self-oscillations and bunching of striations in ionospheric modifications. *Physics Letters, Section A: General, Atomic and Solid State Physics*, *239*(6), 385–392. https://doi.org/10.1016/S0375-9601(98)00006-1

Gurevich, A. V., Zybin, K. P., & Lukyanov, A. V. (1995). Stationary striations developed in the ionospheric modification. *Physical Review Letters*, *75*(13), 2622–2625.

Gustavsson, B., Leyser, T. B., Kosch, M., Rietveld, M. T., Steen, Å., Brändström, B. U. E., & Aso, T. (2006). Electron gyroharmonic effects in ionization and electron acceleration during high-frequency pumping in the ionosphere. *Physical Review Letters*, *97*(19), 1–4. https://doi.org/10.1103/PhysRevLett.97.195002

Hagfors, T., & Lehtinen, M. (1981). Electron temperature derived from incoherent scatter radar observations of the plasma line frequency. *Journal of Geophysical Research*, *86*(A1), 119–124. https://doi.org/10.1029/JA086iA01p00119

Honary, F., Robinson, T., Wright, D., Stocker, A., Rietveld, M., & McCrea, I. (1999). First direct observations of the reduced striations at pump frequencies close to the electron gyroharmonics. *Annales Geophysicae*, *17*, 1235–1238. https://doi.org/10.1007/s00585-999-1235-6

Honary, F., Stocker, A. J., Robinson, T. R., Jones, T. B., & Stubbe, P. (1995). Ionospheric plasma response to HF radio waves operating at frequencies close to the third harmonic of the electron gyrofrequency. *Journal of Geophysical Research*, *100*(A11), 21,489–21,501.

Huang, J., & Kuo, S. P. (1994). A theoretical model for the broad upshifted maximum in the stimulated electromagnetic emission spectrum. *Journal of Geophysical Research*, *99*(A10), 19,569–19,576.

Hunsucker, R. D. (1982). Atmospheric gravity waves generated in the high-latitude ionosphere: A review. *Reviews of Geophysics*, *20*(2), 293–315. https://doi.org/10.1029/RG020i002p00293

Isham, B., Hagfors, T., Mishin, E., Rietveld, M. T., La Hoz, C., Kofman, W., & Leyser, T. B. (1999). A search for the location of the HF excitation of enhanced ion acoustic and langmuir waves with EISCAT and the Tromso Heater. *Radiophysics and Quantum Electronics*, *42*(7), 533–534.

Isham, B., Kofman, W., Hagfors, T., Nordling, J., Thidè, B., LaHoz, C., & Stubbe, P. (1990). New phenomena observed by EISCAT during an RF ionospheric modification experiment. *Radio Science*, *25*(3), 251–262. https://doi.org/10.1029/RS025i003p00251

Isham, B., La Hoz, C., Kohl, H., Hagfors, T., Leyser, T. B., & Rietveld, M. T. (1996). Recent EISCAT heating results using chirped ISR. *Journal of Atmospheric and Terrestrial Physics*, *58*(1-4), 369–383. https://doi.org/10.1016/0021-9169(95)00042-9

Isham, B., Rietveld, M., Hagfors, T., La Hoz, C., Mishin, E., Kofman, W., et al. (1999). Aspect angle dependence of HF enhanced incoherent backscatter. *Advances in Space Research*, *24*(8), 1003–1006. https://doi.org/10.1016/S0273-1177(99)00555-4

Istomin, Y. N., & Leyser, T. B. (1997). Small-scale magnetic field-aligned density irregularities excited by a powerful electromagnetic wave. *Physics of Plasmas*, *4*(3), 817. https://doi.org/10.1063/1.872175

Kelley, M. C., Arce, T. L., Salowey, J., Sulzer, M., Armstrong, W. T., Carter, M., & Duncan, L. (1995). Density depletions at the 10-m scale induced by the Arecibo heater. *Journal of Geophysical Research*, *100*(A9), 17,367–17,376.

Kosch, M. J., Mjlhus, E., Ashrafi, M., Rietveld, M. T., Yeoman, T., & Nozawa, S. (2011). Angular dependence of pump-induced bottomside and topside ionospheric plasma turbulence at EISCAT. *Journal of Geophysical Research*, *116*, A03322. https://doi.org/10.1029/2010JA016014

Kosch, M., Rietveld, M., Kavanagh, A., Davis, C., Yeoman, T., Honary, F., & Hagfors, T. (2002). High-latitude pump-induced optical emissions for frequencies close to the third electron gyro-harmonic. *Geophysical Research Letters*, *29*(23), 2112. https://doi.org/10.1029/2002GL015744

Lehtinen, M. S., & Huuskonen, A. (1996). General incoherent scatter analysis and GUISDAP. *Journal of Atmospheric and Terrestrial Physics*, *58*(1-4), 435–452. https://doi.org/10.1016/0021-9169(95)00047-X

Leyser, T. B. (2001). Stimulated electromagnetic emissions by high-frequency electromagnetic pumping of the ionospheric plasma. *Space Science Reviews*, *98*(3-4), 223–328. https://doi.org/10.1023/A:1013875603938

Leyser, T. B., James, H. G., Gustavsson, B., & Rietveld, M. T. (2018). Possible evidence of L-mode electromagnetic wave pumping of ionospheric plasma in geomagnetic zenith. *Annales Geophysicae*, *36*(900), 167. https://doi.org/10.1029/2009GL041438

Leyser, T. B., & Nordblad, E. (2009). Self-focused radio frequency L wave pumping of localized upper hybrid oscillations in high-latitude ionospheric plasma. *Geophysical Research Letters*, *36*, L24105. https://doi.org/10.1029/2009GL041438

Leyser, T. B., Thidè, B., Derblom, H., Hedberg, Å., Lundborg, B., Stubbe, P., & Kopka, H. (1989). Stimulated Electromagnetic Emission near Electron Cyclotron Harmonics in the Ionosphere. *Physical Review Letters*, *66*(11), 1441–1443. https://doi.org/10.1103/PhysRevLett.21.1441

Leyser, T. B., & Wong, A. Y. (2009). Powerful electromagnetic waves for active environmental research in geospace. *Reviews of Geophysics*, *47*, RG1001. https://doi.org/10.1029/2007RG000235

Mishin, E., Hagfors, T., & Isham, B. (2001). A generation mechanism for topside enhanced incoherent backscatter during high frequency modification experiments in Tromsø. *Geophysical Research Letters*, *28*(3), 479–482. https://doi.org/10.1029/2000GL000122

Mjølhus, E. (1990). On linear conversion in a magnetized plasma. *Radio Science*, *25*(6), 1321–1339.

Mjølhus, E. (1993). On the small scale striation effect in ionospheric radio modification experiments near harmonics of the electron gyro frequency. *Journal of Atmospheric and Terrestrial Physics*, *55*(6), 907–918. https://doi.org/10.1016/0021-9169(93)90030-3

Mjølhus, E., & Flå, T. (1984). Direct access to plasma resonance in ionospheric radio experiments. *Journal of Geophysical Research*, *89*(A6), 3921–3928.

Nordblad, E., & Leyser, T. B. (2010). Ray tracing analysis of L mode pumping of the ionosphere, with implications for the magnetic zenith effect. *Annales Geophysicae*, *28*(9), 1749–1759. https://doi.org/10.5194/angeo-28-1749-2010

Rietveld, M. T., Isham, B., Grydeland, T., La Hoz, C., Leyser, T. B., Honary, F., et al. (2002). HF-pump-induced parametric instabilities in the auroral E-region. *Advances in Space Research*, *29*(9), 1363–1368. https://doi.org/10.1016/S0273-1177(02)00186-2

Rietveld, M. T., Kohl, H., Kopka, H., & Stubbe, P. (1993). Introduction to ionospheric heating at Tromsø-I. Experimental overview. *Journal of Atmospheric and Terrestrial Physics*, *55*(4-5), 577–599. https://doi.org/10.1016/0021-9169(93)90007-L

Rietveld, M. T., Kosch, M. J., Blagoveshchenskaya, N. F., Kornienko, V. A., Leyser, T. B., & Yeoman, T. K. (2003). Ionospheric electron heating, optical emissions, and striations induced by powerful HF radio waves at high latitudes: Aspect angle dependence. *Journal of Geophysical Research*, *108*(A4), 1–16. https://doi.org/10.1029/2002JA009543

Rietveld, M. T., Senior, A., Markkanen, J., & Westman, A. (2016). New capabilities of the upgraded EISCAT high-power HF facility. *Radio Science*, *51*, 1533–1546. https://doi.org/10.1002/2016RS006093

Robinson, T. R. (1989). The heating of the high latitude ionosphere by high power radio waves. *Physics Reports*, *179*(2 - 3), 79–209.

Robinson, T. R., Honary, F., Stocker, A. J., Jones, T. B., & Stubbe, P. (1996). First EISCAT observations of the modification of F-region electron temperatures during RF heating at harmonics of the electron gyro frequency. *Journal of Atmospheric and Terrestrial Physics*, *58*(1-4), 385–395. https://doi.org/10.1016/0021-9169(95)00043-7

Showen, R. L., & Behnke, R. A. (1978). The effect of HF-induced plasma instabilities on ionospheric electron temperatures. *Journal of Geophysical Research*, *83*(A1), 207–209.

Stubbe, P. (1996). Review of ionospheric modification experiments at Tromsø. *Journal of Atmospheric and Terrestrial Physics*, *58*(1-4), 349–368. https://doi.org/10.1016/0021-9169(95)00041-0

Stubbe, P., Kohl, H., & Rietveld, M. T. (1992). Langmuir turbulence and ionospheric modification. *Journal of Geophysical Research*, *97*(A5), 6285–6297.

Stubbe, P., Stocker, A. J., Honary, F., Robinson, T. R., & Jones, T. B. (1994). Stimulated electromagnetic emissions an anomalous HF wave absorption near electron gyroharmonics. *Journal of Geophysical Research*, *99*(A4), 6233–6246.

Thidè, B., Sergeev, E. N., Grach, S. M., Leyser, T. B., & Carozzi, T. D. (2005). Competition between Langmuir and upper-hybrid turbulence in a high-frequency-pumped ionosphere. *Physical Review Letters*, *95*(25), 1–4. https://doi.org/10.1103/PhysRevLett.95.255002

Tjulin, A. (2017). EISCAT Experiments, EISCAT Scientific Association, (March).

Utlaut, W. F., & Violette, E. J. (1974). A summary of vertical incidence radio observations of ionospheric modification. *Radio Science*, *9*(11), 895–903. https://doi.org/10.1029/RS009i011p00895

Vas'kov, V. V., Bud'ko, N. I., Kapustina, O. V., Mikhailov, Y. M., Ryabova, N. A., Komrakov, G. P., et al. (1995). Appearance of VLF and ELF-noises in topside ionosphere under the action of high power radio wave from data of satellite intercosmos-24. *Advances in Space Research*, *15*(12), 49–56. https://doi.org/10.1016/0273-1177(95)00011-3

Vas'kov, V. V., & Gurevich, A. V. (1977). Resonance instability of small-scale plasma perturbations. *Journal of Experimental and Theoretical Physics*, *46*(3), 487–494.

Vodyanitskij, A., Erokhin, N. S., Lisitchenko, V., Moiseev, S. S., & Oraevskij, V. (1974). "Transillumination" of the wave barriers in a plasma as a result of kinetic effects. *Nuclear Fusion*, *14*, 267–275.